

Uncertainty quantification of satellite precipitation estimation and Monte Carlo assessment of the error propagation into hydrologic response

Yang Hong,^{1,2} Kuo-lin Hsu,¹ Hamid Moradkhani,¹ and Soroosh Sorooshian¹

Received 30 June 2005; revised 9 March 2006; accepted 28 March 2006; published 12 August 2006.

[1] The aim of this paper is to foster the development of an end-to-end uncertainty analysis framework that can quantify satellite-based precipitation estimation error characteristics and to assess the influence of the error propagation into hydrological simulation. First, the error associated with the satellite-based precipitation estimates is assumed as a nonlinear function of rainfall space-time integration scale, rain intensity, and sampling frequency. Parameters of this function are determined by using high-resolution satellite-based precipitation estimates and gauge-corrected radar rainfall data over the southwestern United States. Parameter sensitivity analysis at 16 selected $5^\circ \times 5^\circ$ latitude-longitude grids shows about 12–16% of variance of each parameter with respect to its mean value. Afterward, the influence of precipitation estimation error on the uncertainty of hydrological response is further examined with Monte Carlo simulation. By this approach, 100 ensemble members of precipitation data are generated, as forcing input to a conceptual rainfall-runoff hydrologic model, and the resulting uncertainty in the streamflow prediction is quantified. Case studies are demonstrated over the Leaf River basin in Mississippi. Compared with conventional procedure, i.e., precipitation estimation error as fixed ratio of rain rates, the proposed framework provides more realistic quantification of precipitation estimation error and offers improved uncertainty assessment of the error propagation into hydrologic simulation. Further study shows that the radar rainfall-generated streamflow sequences are consistently contained by the uncertainty bound of satellite rainfall generated streamflow at the 95% confidence interval.

Citation: Hong, Y., K.-L. Hsu, H. Moradkhani, and S. Sorooshian (2006), Uncertainty quantification of satellite precipitation estimation and Monte Carlo assessment of the error propagation into hydrologic response, *Water Resour. Res.*, 42, W08421, doi:10.1029/2005WR004398.

1. Introduction

[2] Precipitation is a key forcing variable to the land surface hydrological process at all space-timescales. Therefore a better understanding of the spatial and temporal distribution of precipitation is critical to water resources management where the sizes of basins range from 100 km^2 to $100,000 \text{ km}^2$ and the temporal integration of rainfall inputs ranges from hours to days. However, precipitation observation from ground-based radar or gauge measurement for the remote areas and mountain regions is very limited. Recent development of satellite-based precipitation-retrieval techniques has been providing extended precipitation coverage beyond ground in situ data [Adler *et al.*, 2003; Ba and Gruber, 2001; Bellerby *et al.*, 2000; Hong *et al.*, 2004, 2005; Hsu *et al.*, 1997; Huffman *et al.*, 2001; Joyce *et al.*, 2004; Kuligowski, 2002; Kidd *et al.*, 2003; Miller *et al.*,

2001; Sorooshian *et al.*, 2000; Xie *et al.*, 2003]. While these algorithms provide precipitation products at spatial and temporal scales relevant to atmospheric and hydrological applications, quantification of the estimation error associated with the products at a range of space scales and timescales is critical due to the emerging use of satellite precipitation products in the study of hydrologic and water management applications. A great deal of progress in evaluating rainfall estimation error has been made over the past decades [Anagnostou *et al.*, 1999; Carpenter and Georgakakos, 2004; Ciach *et al.*, 2003; Huffman, 1997; Hossain *et al.*, 2004; Hossain and Anagnostou, 2004; Krajewski *et al.*, 1991, 2000; Krzysztofowicz, 1999; Li *et al.*, 1996, 1998; McCollum and Krajewski, 1998; Rudolf, 1993; Steiner *et al.*, 1999; Steiner, 1996; Steiner *et al.*, 2003]. In one of those studies, Huffman [1997] developed a statistical relationship of the root-mean-square random errors associated with precipitation estimates. Ciach and Krajewski [1999] proposed the error variance separation (EVS) method to decompose the uncertainty of reference error into retrieval error and sampling error. Gebremichael *et al.* [2003] assessed the key factors, such as gauge density and sampling size, that affect the accuracy of EVS results. Steiner *et al.* [2003] proposed a framework to identify possible relationships between sampling error in radar

¹Center for Hydrometeorology and Remote Sensing, Department of Civil and Environmental Engineering, University of California, Irvine, California, USA.

²Now at NASA Goddard Space Flight Center, Greenbelt, Maryland, USA.

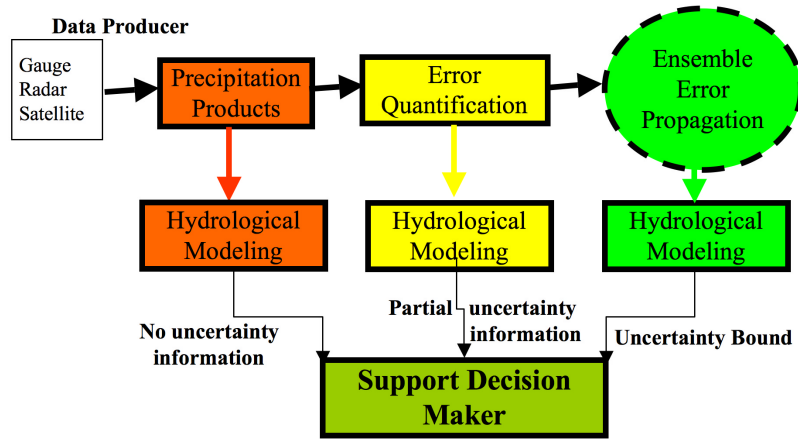


Figure 1. A conceptual “end-to-end” error analysis framework for precipitation data producers and users.

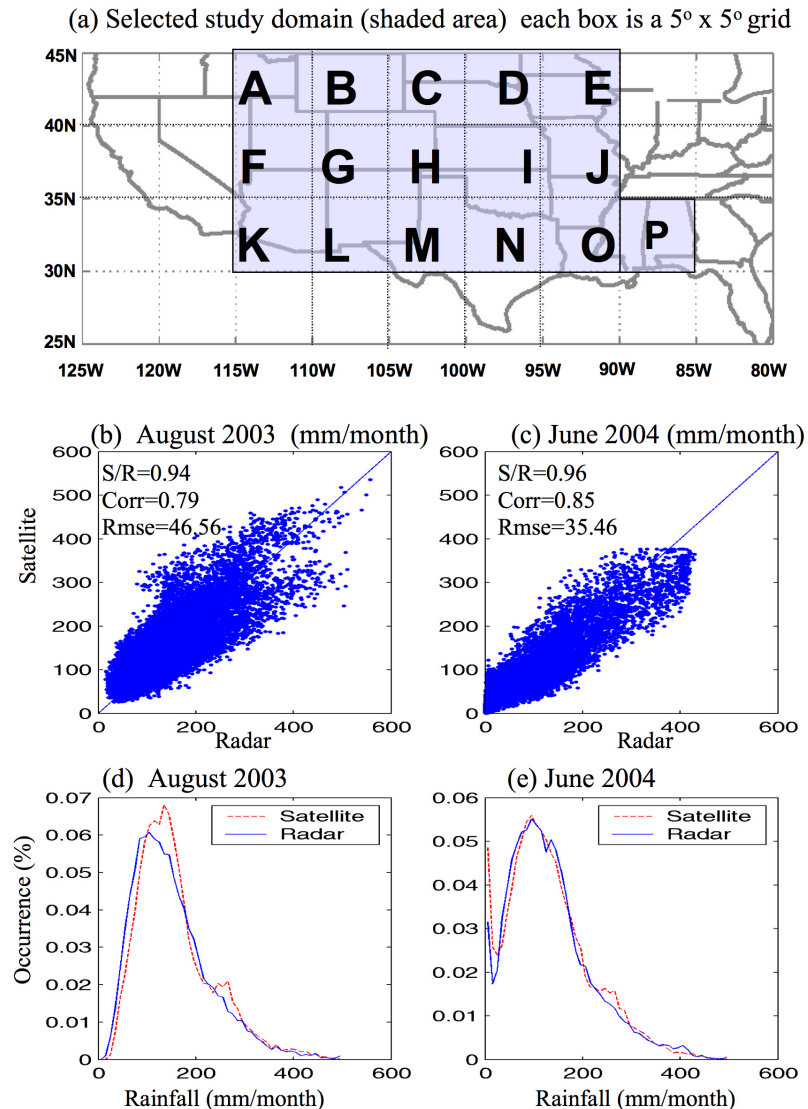


Figure 2. (a) Geographic domain and satellite-based versus radar-based accumulated monthly rainfall over all selected boxes in (b) August 2003 and (c) June 2004; and (d-e) the occurrence of monthly rainfall for the 2 months. Note that the S/R is the ratio of satellite versus radar rainfall, Corr is correlation coefficient, and RMSE is the root-mean-square error.

Table 1. Reference Error $\sigma/\hat{R}(\%)$ at a Range of Spatiotemporal Scales at Box M in June 2004^a

	0.04°	0.12°	0.24°	0.48°	0.96°
1 hour	1.1269	1.065	0.984	0.839157	0.782346
3 hours	0.9457	0.925	0.867	0.813293	0.735735
6 hours	0.8761	0.871	0.825	0.741898	0.698290
12 hours	0.8316	0.833	0.790	0.732958	0.692426
24 hours	0.7866	0.785	0.758	0.703407	0.675744

^aSee Figure 2a.

rainfall estimates and several other factors. *Hossain et al.* [2004] conducted a sensitivity analysis to understand the implication of satellite Passive Microwave (PM) rainfall retrieval and sampling error on flood prediction uncertainty for medium-sized ($\sim 100 \text{ km}^2$) watersheds. In a follow-up paper, *Hossain and Anagnostou* [2004] examined the passive microwave (PM)- and infrared (IR)-based satellite rainfall retrieval for flood prediction using a probabilistic error model. *Hossain and Anagnostou* [2004] also explored the uncertainty bound of simulated flood events based on various microwave rainfall samples and hourly infrared-based rainfall estimates. The above research indicated that it is critical to improve the communication between precipitation data producer and user community by quantifying the estimation error and assessing the influence of error propagation into hydrologic processes. For data providers, the error inherent in the retrieval algorithm is of particular interest. However, from the perspective of data users, the error associated with the data and the influence of the error propagation into the hydrologic responses is generally interesting. As shown in Figure 1, quantification of error associated with precipitation products would provide more useful information for users (decision makers) than no error assessment at all. To quantify the influence of estimation error on hydrologic responses by ensemble simulation would further place an appropriate degree of confidence from data users' perspectives.

[3] This study aims to foster the development of an end-to-end uncertainty propagation analysis framework that can quantify the error of satellite rainfall estimation and further assess the uncertainty of the error propagation into various hydrological modeling and applications. The error is expressed as a nonlinear multivariate function of space-time integration scale, rain intensity, and sampling frequency. The advantage of this error formula, for example, is that the various users of the precipitation products can approximate the error by simply implementing the function at their specified space-timescales and rain intensities. The influence of precipitation estimation error on a conceptual rainfall-runoff hydrologic model is examined through

Test Site: Box I in August 2003

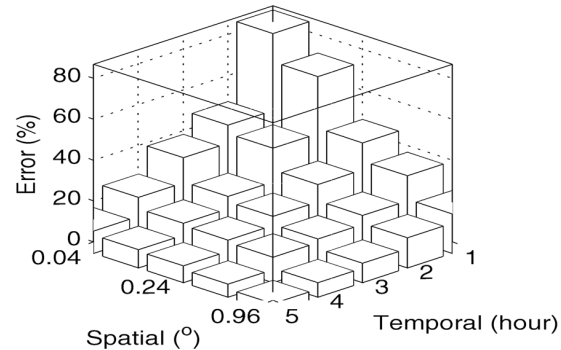


Figure 3. Satellite-based rainfall estimation error distribution as a function of spatial and temporal resolution without consideration of rain intensity.

Monte Carlo simulation. By this approach, an ensemble of precipitation data is generated, as forcing to the hydrologic model, and the resulting uncertainty in the hydrologic response is quantified at different confidence intervals.

[4] The outline of this paper is as follows: The formulation of precipitation estimation error is described in section 2, and the data used in the study and the calibration procedure to approximate the error function are presented in section 3. The uncertainty of streamflow prediction associated with the satellite rainfall estimation error is assessed in section 4, and the summary and discussion are given in section 5.

2. Error Quantification Framework

[5] There is a fundamental difference between satellite and radar remotely sensed observations of precipitation and those measured directly by rain gauges. While satellites and radar measure rainfall as a space integral at a given instance in time, rain gauges, on the other hand, measure rainfall as a time integral of rain at a particular location. Let $r(\mathbf{x}, t)$ represent the rain rate (mm h^{-1}) at a point \mathbf{x} and in time t . Then, the rainfall at point \mathbf{x} accumulated during time period T is

$$R_T(\mathbf{x}) = \frac{1}{T} \int_0^T r(\mathbf{x}, t) dt \quad (1)$$

and the instantaneous rain rate (at time t) averaged over an area of A is

$$R_A(t) = \frac{1}{A} \int_0^A r(\mathbf{x}, t) d\mathbf{x} \quad (2)$$

The $R_A(t)$ is of interest for satellite rainfall estimation because it is the typical measurement by the satellite at each visit. Equation (2) also indicates the nature of the measurements from satellite data: rainfall is the quantity measured as an integral of space (A) at a point in time (t). Integration of the instantaneous rain rate $r(\mathbf{x}, t)$, both in time and space, gives the space-time average of rain rate

$$R_{AT} = \frac{1}{AT} \int_0^T \int_0^A r(\mathbf{x}, t) d\mathbf{x} dt = \frac{1}{T} \int_0^T R_A(t) dt = \frac{1}{A} \int_0^A R_T(\mathbf{x}) d\mathbf{x} \quad (3)$$

Table 2. Number of Grids for the Statistical Computation at Box M in June 2004^a

	0.04°	0.12°	0.24°	0.48°	0.96°
1 hour	10929571	1172898	278442	68965	16787
3 hours	3665026	392174	93145	23048	5524
6 hours	1839258	196388	46657	11539	2733
12 hours	931103	99003	23529	5838	1341
24 hours	462603	48789	11598	2869	666

^aSee Figure 2a.

Table 3. Reference Error $\sigma/\hat{R}(100\%)$ at Various Spatialtemporal Scales and 10 Bins of Incremental Rain Rate^a

Spatial, deg	Rain Rate, mm/h								
	0.1–0.5	0.5–1	1–2	2–3	3–4	4–5	5–10	10–20	>20
<i>1 Hour</i>									
0.04	553.4	283.5	189.3	139.3	111.8	103.1485	99.5772	93.0648	83.686
0.12	370.2	225.8	156.4	127.3	104.7	101.2412	93.03398	90.108	82.135
0.24	263	197.5	131	106.9	98.45	91.29212	86.49507	83.5329	79.156
0.48	233.2	138.7	105.5	93.07	85.2	77.3654	70.61353	70.8495	69.504
0.96	99.13	105.4	79.04	71.11	72.25	71.28587	70.26871	65.4098	-
<i>3 Hours</i>									
0.04	295.2	180.2	125	102.1	93.73	90.52022	86.95734	79.7471	75.879
0.12	229.4	152.6	109.8	98.03	93.1	85.17111	81.61962	78.5683	73.791
0.24	168.6	127.8	105.6	91.78	85.09	80.34503	75.57973	73.4305	73.036
0.48	151.4	102.8	89.69	82.03	71.48	67.73598	70.19385	71.4969	-
0.96	89.1	85.39	75.58	72.87	70.26	64.23749	60.69096	54.8749	-
<i>6 Hours</i>									
0.04	200.2	130	101.6	92.46	86.46	83.27407	77.91234	70.7205	74.324
0.12	171.5	118.7	96.97	88.98	79.59	77.38816	75.14635	70.5529	-
0.24	133.3	110.9	90.09	83.9	75.61	71.0505	69.18679	68.9132	-
0.48	111.1	91.63	82.66	74.61	68.58	65.31336	64.8041	62.5515	-
0.96	84.86	82.8	69.49	60.4	55.8	56.77127	-	-	-
<i>12 Hours</i>									
0.04	167.4	109.3	94.83	83.59	75.16	72.53024	69.59589	69.583	-
0.12	143.5	102.9	88.29	77.19	74.95	71.64718	65.70086	60.075	-
0.24	106.9	93.22	83.55	73.8	74.29	64.39437	59.66018	-	-
0.48	89.76	86.07	75.1	69.58	59.19	56.75801	-	-	-
0.96	80.11	73.26	61.08	61.75	56.31	-	-	-	-
<i>24 Hours</i>									
0.04	121.4	94.71	82.94	71.38	65.25	65.19843	-	-	-
0.12	105.8	87.64	78.46	71.14	69.36	-	-	-	-
0.24	93.4	83.85	70.42	68.2	68.24	-	-	-	-
0.48	80.64	71.41	67.77	61.1	-	-	-	-	-
0.96	78.08	70.31	59.11	58.72	-	-	-	-	-

^aDash indicates no data.

Equation (3) assumes perfect measurement of rainfall over an area A and time period T . Because of the imperfect nature of satellite rainfall estimation algorithms, there is always an error associated with the retrieval of the $R_A(t)$. Here, we denote the rain rate averaged over area A as $\hat{R}_A(t)$. Supposing that the satellite makes N visits over an area A during a time period T , one can write the satellite-derived rainfall at space-time averaged scale as

$$\hat{R}_{AT} = \frac{1}{N} \sum_{i=1}^N \hat{R}_A(t_i) = \frac{\Delta t}{T} \sum_{i=1}^{T/\Delta t} \hat{R}_A(t_i) \quad (4)$$

where $\Delta t (= T/N)$ is the time interval between consecutive visits, which is also called sampling frequency. The error associated with \hat{R}_{AT} can be written as

$$\begin{aligned} \varepsilon &= \hat{R}_{AT} - R_{AT} = \frac{1}{N} \sum_{i=1}^N \hat{R}_A(t_i) - R_{AT} \\ &= \frac{\Delta t}{T} \sum_{i=1}^{T/\Delta t} \hat{R}_A(t_i) - \frac{1}{T} \int_0^T R_A(t) dt \end{aligned} \quad (5)$$

In reality, there are no “true data” available. The approximation of the “true error ε ” can be assessed through

comparison with independent reference data (R_{AT}^{ref} , e.g., radar or gauge rainfall). The reference error is often used to approximate the true error (ε) (see Appendix A for an explanation). Both the standard deviation and the variance are measures of spread of the reference error (ε). The standard deviation is the square root of the variance and has the desirable property of being in the same units as the data. That is, in the case of this study, both rainfall rate and its error standard deviation are in mm h^{-1} :

$$\sigma_E = \sqrt{\text{Var}(\hat{R}_{AT} - R_{AT}^{\text{ref}})} = \sqrt{\text{Var}\left(\frac{\Delta t}{T} \sum_{i=1}^{T/\Delta t} \hat{R}_A(t_i) - R_{AT}^{\text{ref}}\right)} \quad (6)$$

The error of precipitation estimate, σ_E , is a function of its area coverage (A), time integration (T), sampling frequency (Δt), and the space-time average of rain rate (\hat{R}), inversely proportional to A and T and nonlinearly proportional to Δt (sampling frequency) and \hat{R} . In this study, similar to *Steiner et al. [2003]*, the area A is substituted with spatial scale L , the side length of A . Thus the nonlinear multivariate function random error, σ_E , is written as

$$\sigma_E = f\left(\frac{1}{L}, \frac{\Delta t}{T}, \hat{R}\right) = a\left(\frac{1}{L}\right)^b \left(\frac{\Delta t}{T}\right)^c \left(\hat{R}\right)^d \quad (7)$$

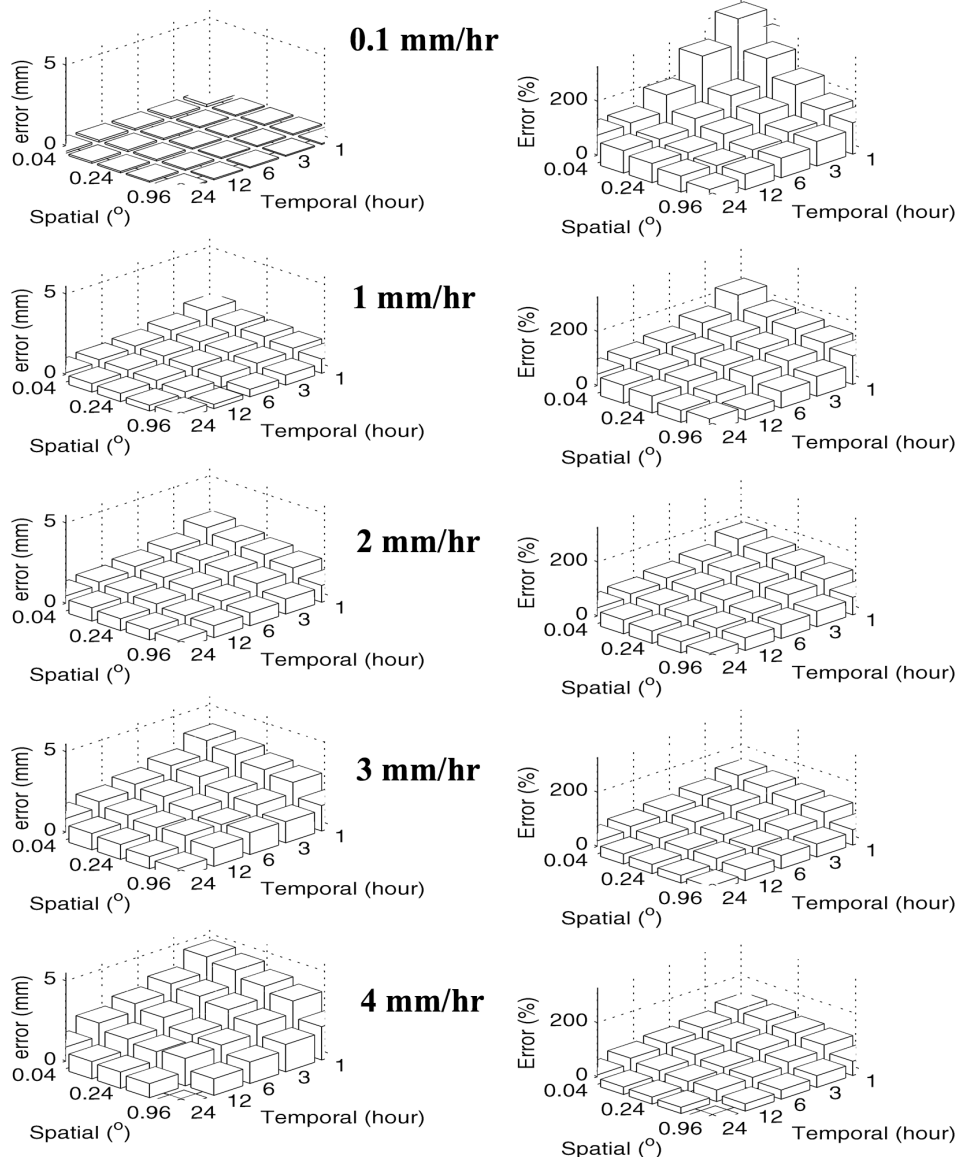


Figure 4. (left) Error distribution as a function of spatial and temporal scales at increasing rain rates for box I (August 2003). (right) Percentage of error to rain rate.

where a , b , c , and d are the parameters of the approximation function, and the units of L , T , and \hat{R}_{AT} are degrees of longitude, hour, and mm h^{-1} , respectively. The sampling frequency Δt is 1 hour from the satellite observation in this study. In order to make it comparable to results obtained from different climate regimes and various seasons, e.g., dry or wet, the error σ_E needs to be tied to a rain rate. As shown in equation (8), the error could also be expressed as percentage (%) of rain rate by dividing the space-time average of rain rate (\hat{R}):

$$(\sigma_E/\hat{R}) = f\left(\frac{1}{L}, \frac{\Delta t}{T}, \hat{R}\right) = a\left(\frac{1}{L}\right)^b \left(\frac{\Delta t}{T}\right)^c (\hat{R})^{d-1} \quad (8)$$

3. Data and Analysis Procedure

3.1. Data

[6] The satellite rainfall estimates used in this study are from the PERSIANN-CCS (Precipitation Estimation

from Remote Sensed Information using Artificial Neural Network–Cloud Classification System) algorithm [Hong *et al.*, 2004]. The PERSIANN-CCS is the follow-up version of our earlier reported work, the PERSIANN algorithm [Hsu *et al.*, 1997; Sorooshian *et al.*, 2000]. The PERSIANN-CCS is a patch-based cloud classification and rainfall estimation system based on coregistered passive microwave and infrared images from low Earth-orbiting and geostationary satellites by using computer image processing and pattern recognition techniques. We operate this system (<http://hydus.eng.uci.edu/CCS/>) with the goal of producing data at spatial-temporal resolution (reaching $4 \times 4 \text{ km}^2$ 30 min) suitable for basin-scale hydrological research and applications. PERSIANN-CCS has been generating precipitation estimates at resolution ($0.04^\circ \times 0.04^\circ$ scale and 30-min time interval) since 2000.

[7] The National Weather Service WSR-88D stage IV data serve as ground reference rainfall data at $4 \text{ km} \times 4 \text{ km}$ spatial and hourly temporal resolution. Both stage II and

Table 4. Parameter Estimation for Each of the 16 Selected Boxes

Boxes	<i>a</i>	<i>b</i>	<i>c</i>	<i>d</i>	RMSE, %
A	1.11	0.2608	0.328	0.682595	14.0912
B	0.9794	0.2751	0.3423	0.696877	10.57958
C	0.8791	0.2274	0.3447	0.549421	17.07047
D	0.7279	0.193	0.3103	0.515032	12.9689
E	0.842	0.3051	0.3724	0.727115	12.99048
F	0.9755	0.2205	0.2878	0.642486	15.42445
G	0.9451	0.2865	0.3538	0.708498	13.80694
H	0.9241	0.192	0.2593	0.613987	16.25296
I	0.8674	0.1962	0.2635	0.618213	14.82851
J	0.7842	0.294	0.3613	0.715968	13.69446
K	0.9274	0.1774	0.2154	0.965651	10.66329
L	0.9659	0.2577	0.325	0.795838	10.00643
M	0.7211	0.2136	0.3309	0.5356	15.76622
N	0.9703	0.3406	0.4078	0.762369	14.0912
O	0.7492	0.3115	0.4288	0.633527	16.54722
P	0.6854	0.1986	0.3159	0.52057	13.58956
All	0.8018	0.2317	0.3465	0.5576	9.5
Maximum	1.1100	0.3400	0.4288	0.9657	17.0100
Minimum	0.6854	0.1774	0.2154	0.5150	9.5000
Range	0.4246	0.1632	0.2135	0.4506	7.5705
Mean	0.8732	0.2460	0.3290	0.6618	13.6395
Median	0.8791	0.2317	0.3309	0.6425	13.8069
STD	0.1166	0.0496	0.0529	0.1161	2.3190
Variance	0.0136	0.0025	0.0028	0.0135	5.3780

stage IV analysis are national products generated at National Center for Environmental Prediction (NCEP) from multi-sensor (radar and gauge) hourly/6 hourly rainfall data on local 4-km polar stereographic grids. The stage IV data differ from the NCEP stage II data because the NCEP stage II data contain no manual quality control (QC), while the stage IV data benefit from manual QC performed at the

12 River Forecasting Centers over the continental United States. The period of stage IV record begins 1 January 2002, while stage II began to be archived at NCAR on 1 May 1996. The stage IV high spatial and temporal resolution rainfall analysis provides data useful for testing of satellite rainfall estimation algorithms. Additional information about the NCEP stage IV analysis can be found at <http://www.t.emc.ncep.noaa.gov/mmb/ylin/pcpanl/stage4/>.

[8] The selected study coverage, shown in Figure 2a as the shaded area, was divided into 16 boxes, $5^\circ \times 5^\circ$ for each. Two heavy rainfall seasons (August 2003 and June 2004) were selected for the analysis of uncertainty σ_E . The scatterplots of PERSIANN-CCS and radar monthly accumulation rainfall (0.04° grid) during August 2003 and June 2004, respectively, are shown in Figures 2b and 2c. Both months show high spatial correlation (Corr) and relatively low root-mean-square error (RMSE); however, PERSIANN-CCS underestimates the two summer months with satellite-to-radar ratio (S/R) of 0.94 and 0.96, respectively. The occurrence of the rainfall for the two months, respectively, is displayed in Figures 2d and 2e. The peaks of occurrence indicate that both months received relatively heavy rainfall over large areas. In August 2003, the PERSIANN-CCS estimates match the radar at low rainfall regions (less than 100 mm) but overestimates rainfall at medium rainfall (100–200 mm) and heavy rainfall regions (>230 mm). In June 2004, false alarms occur at no rain or light rainfall regions and slightly underestimate at heavy rainfall regions (>350 mm).

3.2. Case Studies

[9] Given their processed basic resolution ($0.04^\circ \times 0.04^\circ$ and hourly), both the satellite and radar data sets were aggregated into a range of discrete temporal (1, 3, 6, 12, and

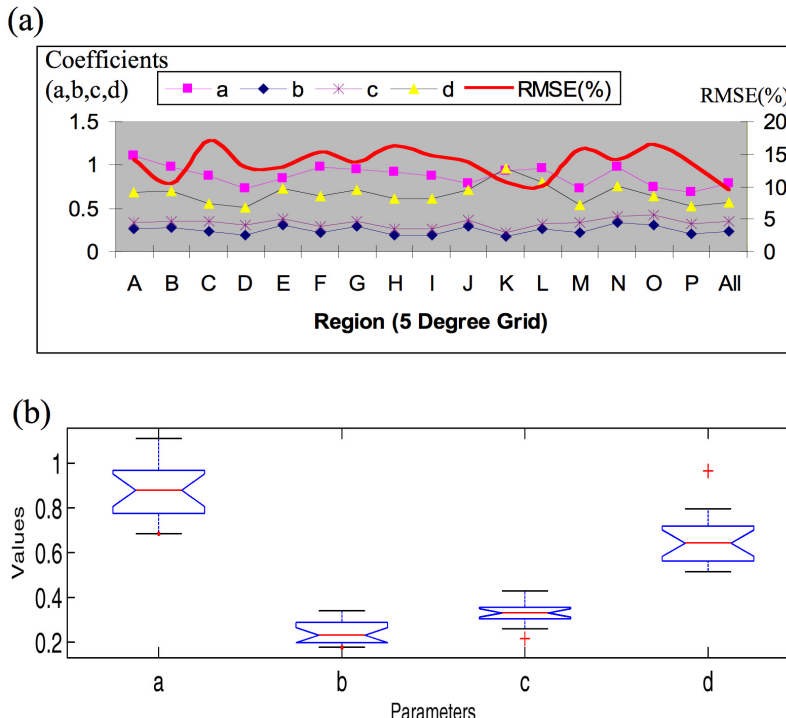


Figure 5. (a) Estimated parameters in equation (7) from the data of each of the selected boxes (A-P) and the data of all the boxes (all) (see Figure 2a and Table 4 for detail) and (b) box plot of the four parameters.

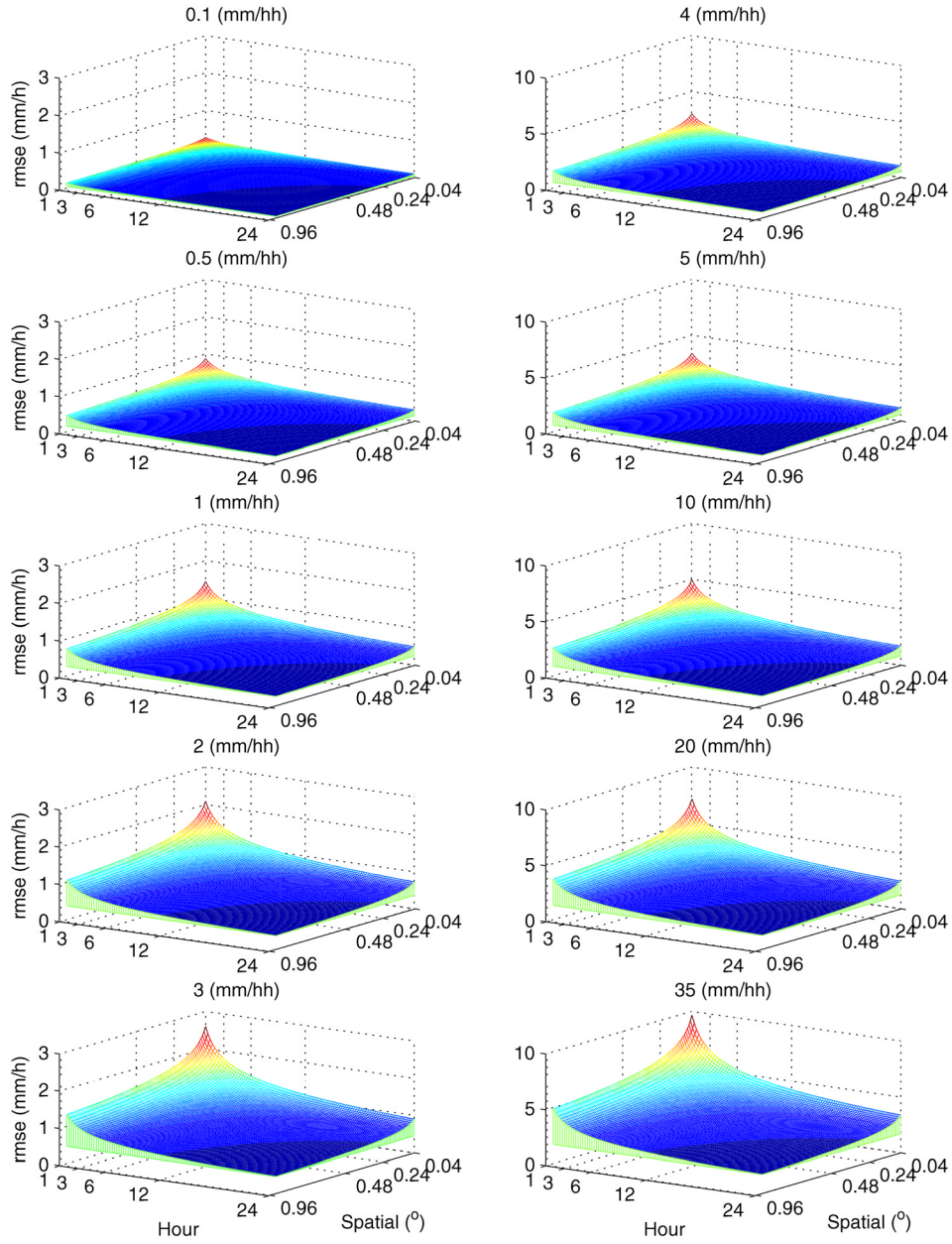


Figure 6. Plot of the error distribution with respect to L , T , and R using the optimal parameters from equation (9).

24 hours) and spatial (0.04° , 0.12° , 0.24° , 0.48° , and 0.96°) scales. Therefore each box is divided into subgrids with side lengths of 0.04° , 0.12° , 0.24° , 0.48° , and 0.96° latitude-longitude; each subgrid holds rainfall intensities at time resolutions of 1, 3, 6, 12, and 24 hour for this analysis. The error analysis is conducted for each box separately. As an example, box I (August 2003) and box M (June 2004), as shown in Figure 2a, were selected to calculate the reference error. Note that the sampling frequency Δt is 1 hour from the PERSIANN-CCS data.

3.2.1. Calculating the Reference Error as a Function of Spatial and Temporal Scales

[10] Regardless of the rainfall intensities, Table 1 shows the reference error $\sigma/\hat{R}(\%)$ as a function of spatial and

temporal scales at box M, the Rio Grande basin, in June 2004 wet season. The count of effective subgrid numbers from this statistical computation is listed in Table 2. The maximum count of a subgrid number at 1-hour 0.04° scale is 11,250,000 ($125 \text{ rows} \times 125 \text{ columns} \times 24 \text{ hour} \times 30 \text{ day}$) within each 5° grid for rainfall data in June 2003. Similarly, the reference error (%) distribution, calculated at box I in August 2003, as a discrete function of spatial and temporal scales is shown in Figure 3. Without consideration of the rain intensity, Table 1 and Figure 3 show that the satellite rainfall estimation reference error (%) is a function of spatial and temporal scales where higher spatial and temporal resolution is subject to larger reference error.

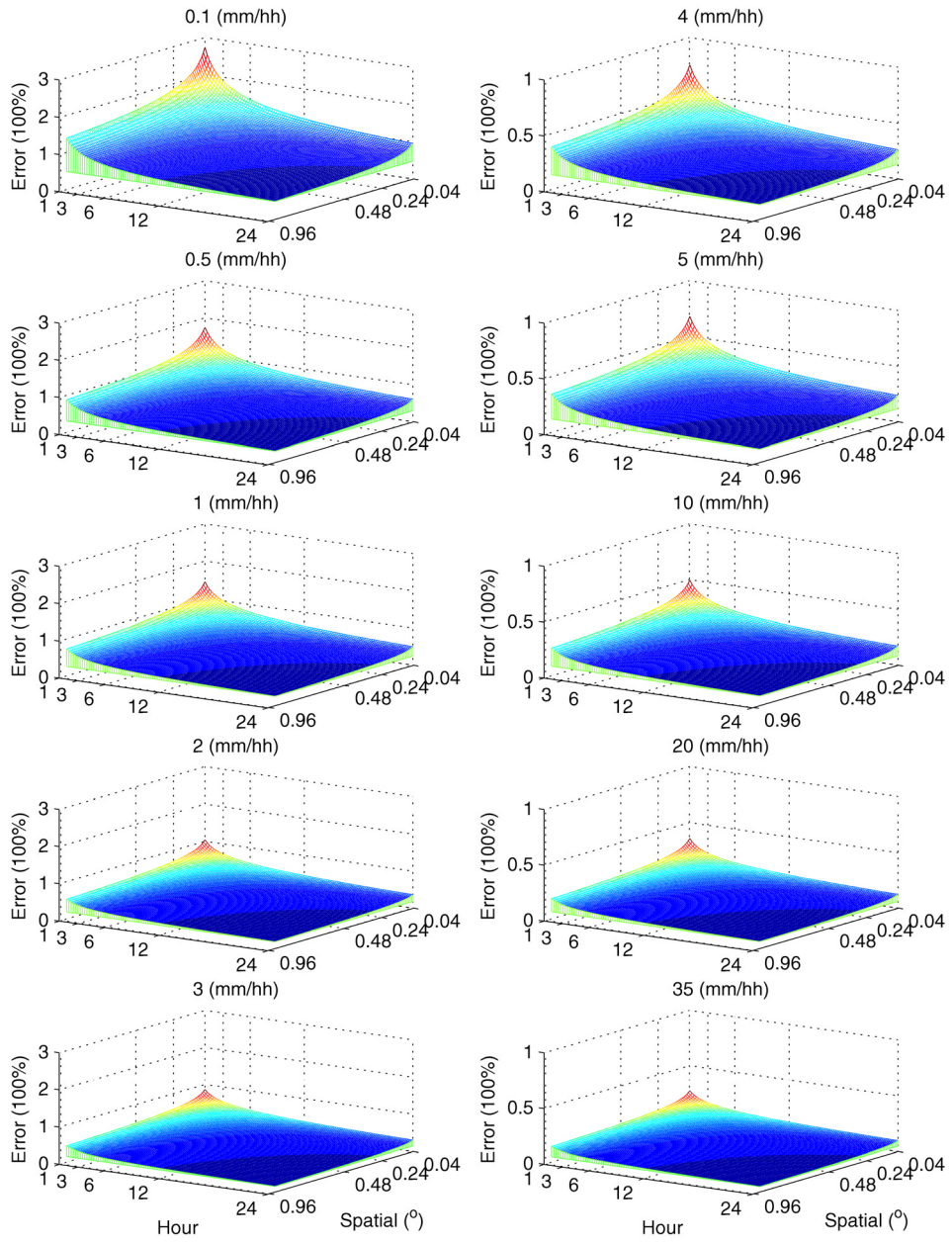


Figure 7. Same as Figure 6, except the error is expressed as percentage (%) of rain rates.

3.2.2. Calculating the Reference Error as a Function of Spatial-Temporal Scales and Rainfall Intensities

[11] The satellite rainfall estimates were incrementally divided into 10 bins according to their intensities; the reference errors are then calculated for each rain rate bin at various spatial and temporal scales. The reference error, derived from box M in June 2004, as a function of both spatial-temporal scales and rainfall intensities is given in Table 3.

[12] The reference error (σ_E) distribution at the discrete temporal and spatial scales and increasing rain rates for box I in August 2003 are displayed in Figure 4 (left). The same reference error is shown in Figure 4 (right), but as a percentage of rainfall estimates $\sigma_E/\hat{R}(\%)$.

[13] The procedure was repeated for the other 14 grids in Figure 2a. A reference error look-up table, similar to Table 3,

is established by using the whole year data (July 2003 to June 2004) for each grid shown in Figure 2a. All the results (not shown here) support the assumption that the error in satellite-based rainfall estimation is inversely proportional to the area and time interval integration and proportional to the rainfall rate.

3.3. Regression Parameter Estimation

[14] For each box shown in Figure 2a, we built up a reference error look-up table from an entire year data set at various spatial-temporal scales and 10 bins of incremental rain intensities. By defining the minimum satellite sampling frequency as 1 hour ($\Delta t = 1$), the parameters (a , b , c , and d) of equation (7) were calibrated using the error look-up table derived from the 1-year data set for every box. The resulting parameter estimates of equation (7) for each of the 16 grids

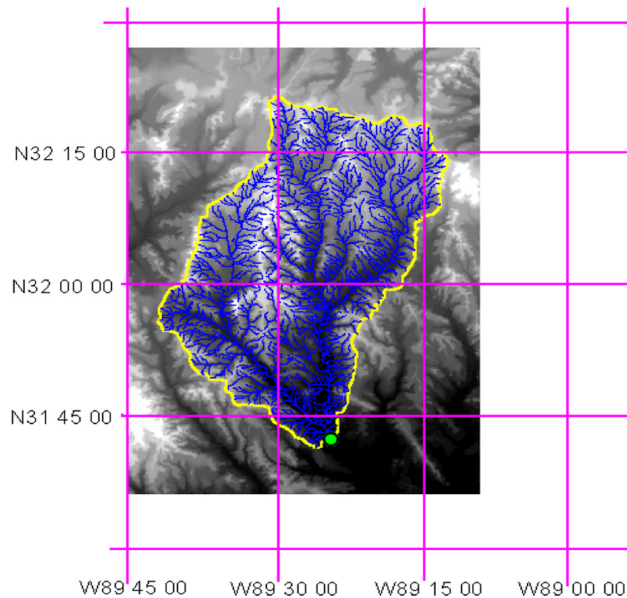


Figure 8. Study area for streamflow uncertainty estimation associated with rainfall uncertainty.

(Figure 2a) and for the data from all of the boxes are listed in Table 4. Using the RMSE as calibration criterion for equation (7), the optimal parameter sets are estimated separately for the data in each $5^\circ \times 5^\circ$ grid box (see Figure 2a). As shown in Figure 5a, the error estimation function with the optimal parameter set is

$$\sigma_E = f\left(\frac{1}{L}, \frac{\Delta t}{T}, \hat{R}\right) = 0.8018 \left(\frac{1}{L}\right)^{0.2317} \left(\frac{1}{T}\right)^{0.3465} (\hat{R})^{0.5576} \quad (9)$$

[15] The box plots of the calibrated parameters are given in Figure 5b. The lower and upper lines of the box are the 25th and 75th percentiles of the sample. The distance between the top and bottom of the box is the interquartile range. The cross sign indicates potential outlier or extreme points of the range; the line in the middle of the box represents the mean. If the mean is not centered in the box, the distribution is skewed. The statistical information of the 17 sets of parameters is also listed in the bottom rows of Table 4. Figure 5 and Table 4 show the spatial variability of each parameter derived from different $5^\circ \times 5^\circ$ latitude-longitude grids. In particular for parameters b , c , and d , the ranges of values are more than 50% of their mean values, which shows that the error of satellite-derived precipitation estimates can be region-dependent. Notably, it is reasonable to expect that the error in wet season is generally larger than dry season. For example in box M, the error simulated from the parameter set in Table 4 is generally smaller than the error in Table 3. The difference essentially originates from the fact that the parameters in Table 4 are calibrated by entire year data [2004], whereas Table 3 represents the error in wet season only (June 2004). Additionally, the parameter fitting is influenced by the uneven distribution of the rainfall intensity, more heavy rainfall occurrence in wet season than dry season.

[16] Using the calibrated optimal parameter set in equation (9), Figure 6 plots the reference error estimates (σ_E) with respect to spatial-temporal scales and rainfall intensities; the same reference error estimates but as a percentage of rainfall intensity (σ_E/\hat{R}) are plotted in Figure 7. Note that in the current study, we arguably assume that the effect of sampling frequency in equation (7) is negligible because the PERSIANN-CCS has relatively high sampling frequency (30-min), one of the advantages of rainfall estimates using multiple satellites.

4. Propagation of Rainfall Estimation Error Into Hydrological Response

[17] As the key forcing variable of hydrological processes, the precipitation is largely responsible for the variability in

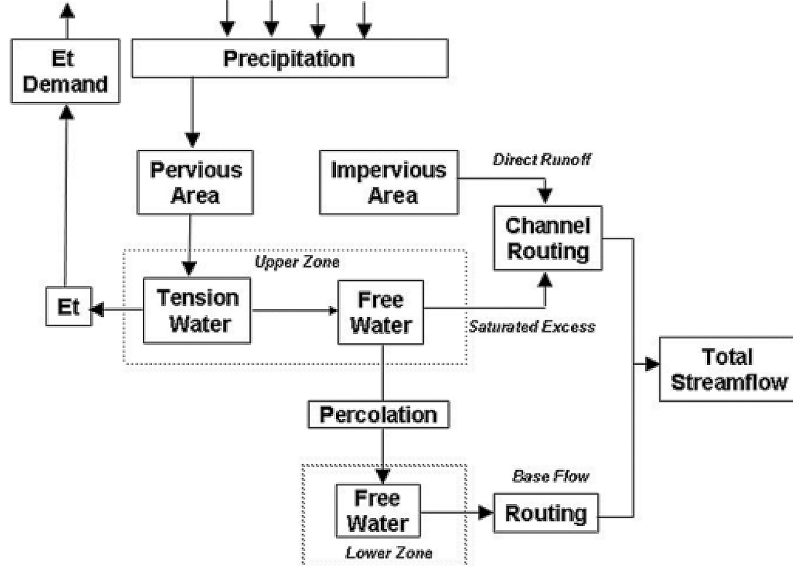


Figure 9. Hydrologic Model (HyMOD) after Boyle et al. [2001].

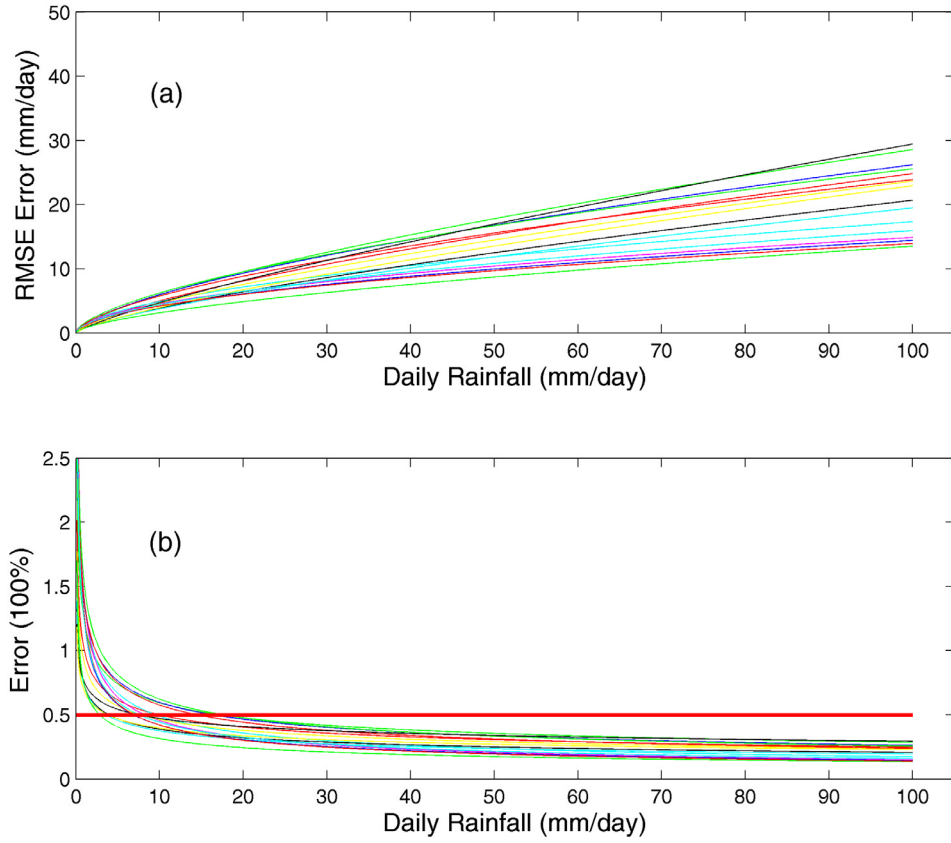


Figure 10. Given the size of the Leaf River basin and the temporal resolution (daily in this case), the reference error (%) is a function of rain rates according to the error equation (9): (a) the error estimation using the 17 parameter sets listed in Table 4 and (b) same but the error expressed as percentage of rain rates. Note that the straight bold line in Figure 10b indicates the fixed reference error as 50% of rain rates.

model outputs. Clearly, evaluation of the error associated with precipitation products into model behavior is an indispensable element of improving hydrologic modeling and data assimilation.

[18] In the current study, the influence of the error of input-forcing data, i.e., precipitation, through a conceptual rainfall-runoff hydrologic model to output forecasting uncertainty is evaluated by propagating the approximated PERSIANN-CCS rainfall error estimates with a Monte Carlo simulation approach. This approach generates an ensemble of precipitation data as forcing input to fit to the conceptual rainfall-runoff model, and the resulting uncertainty in the forecasted streamflow is then quantified. The applicability and usefulness of this procedure is demonstrated in the case of the Leaf River basin, located north of Collins, Mississippi. The size of the Leaf River basin is about 1949 km². A map of the Leaf River basin is shown in Figure 8. We have used a daily time step for precipitation input. This may be larger than desirable to capture the hydrologic response. See, e.g., Burges [2003] for a perspective on this issue.

[19] To demonstrate rainfall error propagation through a hydrologic model, we employed a parsimonious conceptual Hydrologic Model (HyMOD) as described by Boyle *et al.* [2001] (Figure 9) in the model simulation. HyMOD has its origins in the probability-distributed moisture model (PDM)

[Moore, 1985], an extension of some of the lumped storage models developed in 1960s, and later to the case of multiple storages representing a spatial distribution of different storage capacities in a watershed. HyMOD is a rainfall excess model defined by a nonlinear tank (representative of the watershed soil moisture content) connected with two series of linear tanks, three identical quick flow tanks (responsible for channel routing) in parallel to a slow flow tank representing the base flow. The model contains five states of variables describing the dynamics of the system along with five parameters which characterize the system and need to be calibrated; for more information, see Moradkhani *et al.* [2005a, 2005b].

[20] Once the spatial size (1949 km²) and the temporal resolution (daily in this case) of the Leaf River basin are specified, the standard error of rainfall as a function of rain rate can be estimated from equation (9). Figure 10 shows the error, in terms of RMSE and relative percentage error, of precipitation based on the regression parameters of those 16 test grid boxes and the averaged parameter set listed in Table 4. As shown in Figure 10a, the RMSE of estimated rainfall is increased with respect to rainfall with higher intensity. In terms of percentage error of estimated precipitation (see Figure 10b), high-intensity rainfall is subjected to lower-percentage relative error. The straight bold line shown in Figure 10b assumes the error as fixed ratio (50%)

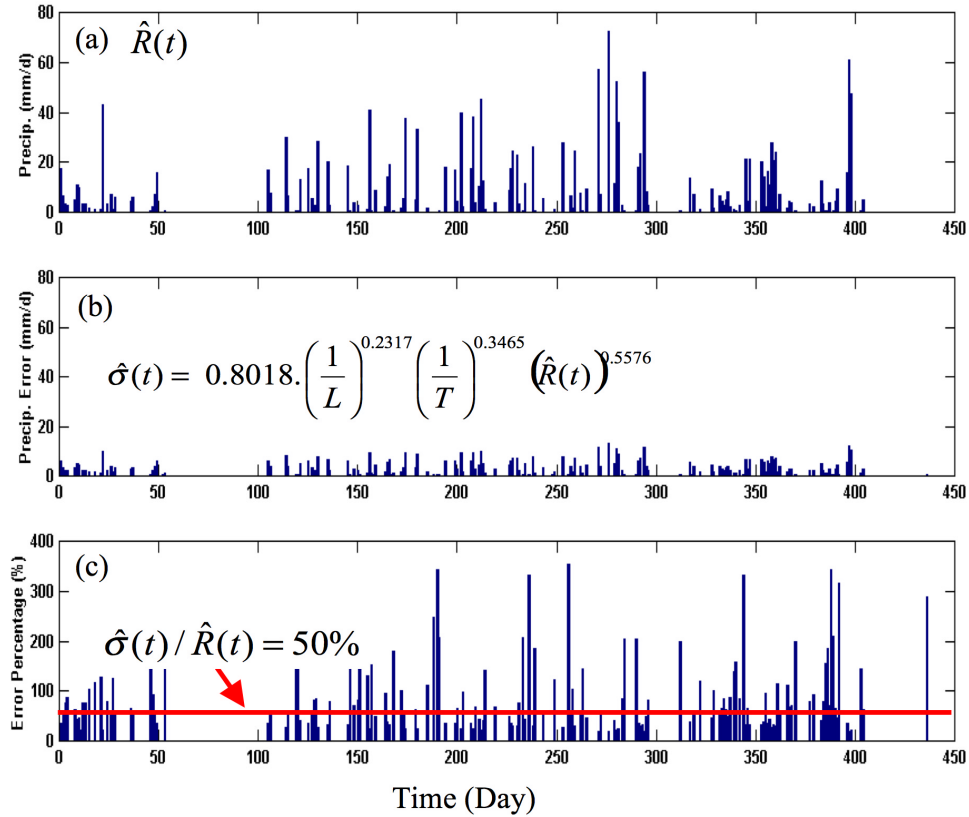


Figure 11. (a) Time series of the daily rainfall over the Leaf River basin; (b) the rainfall estimation error calculated from equation (9); and (c) rainfall error expressed as percentage of rain rates. Note that the straight line in Figure 11c indicates rainfall estimation error as fixed percentage of rainfall intensities, and the bar represents the rainfall error percentage from equation (9).

of rain rates, which is about the average of the rainfall intensity-dependent error, while the true error property of rainfall estimates is unknown. The rain intensity-dependent error reveals more realistic error characteristics of the rainfall data than the fixed ratio method, one of the conventional approaches.

[21] HyMOD streamflow simulation proceeded under two scenarios: (1) the error as a variable ratio of rain rates based on equation (9), and (2) the error as a fixed ratio of rain rates. The satellite daily rainfall estimates over the Leaf River basin for a time period over 1 year are shown in Figure 11a. The daily rainfall error estimated from the scale-dependent function equation (9) is listed in Figure 11b, and the percentage of error to the rain rates is given in Figure 11c. In addition, a fixed ratio of 50% of the daily rain rate error (horizontal line) is also listed as a reference. In each error scenario, 100 ensemble members of the HyMOD simulation were used to derive the confidence interval of streamflow prediction by using the Monte Carlo method. The simulated runoff output and its 95% uncertainty bound derived from the second scenario are displayed in Figure 12a; the results from the first scenario are given in Figure 12b. The red dots represent the runoff time series generated from the satellite rainfall estimates. The results show that the reliability of estimated streamflow is highly related to the intensity of input-forcing data. For both of the error propagation cases, the uncertainty bound is signifi-

cantly higher during high-flow periods and is lower in low-flow regions. However, the 95% uncertainty bound of the simulated runoff as shown in Figure 12b is lower than the one generated from the fixed error ratio case pictured in Figure 12a. The first scenario, scale-dependent error propagation, offers more realistic uncertainty assessment of streamflow prediction than the fixed ratio error propagation, particularly during high flow, i.e., heavy rainfall periods.

[22] Comparison of runoff simulation generated from both stage IV radar precipitation measurement and satellite PERSIANN-CCS measurement is shown in Figure 13. Again, 100 ensemble members were generated from the satellite-based rainfall to derive the streamflow responses. The result of the 66% confidence interval of generated streamflow is listed in Figure 13a, while the 95% confidence interval is listed in Figure 13b. The red dots represent the streamflow sequence generated from radar rainfall, while the solid line shows the synthetic mean of ensemble streamflows simulated from satellite rainfall estimates. At the 66% confidence interval, part of the radar-generated streamflow are not covered by the uncertainty bound, while under the 95% confidence interval, the radar-generated streamflow are consistently contained by the uncertainty bound of satellite-simulated flow. However, the uncertainty bound for the high flow period can be large, as the upper bound can be 100% ~ 300% higher than the radar-

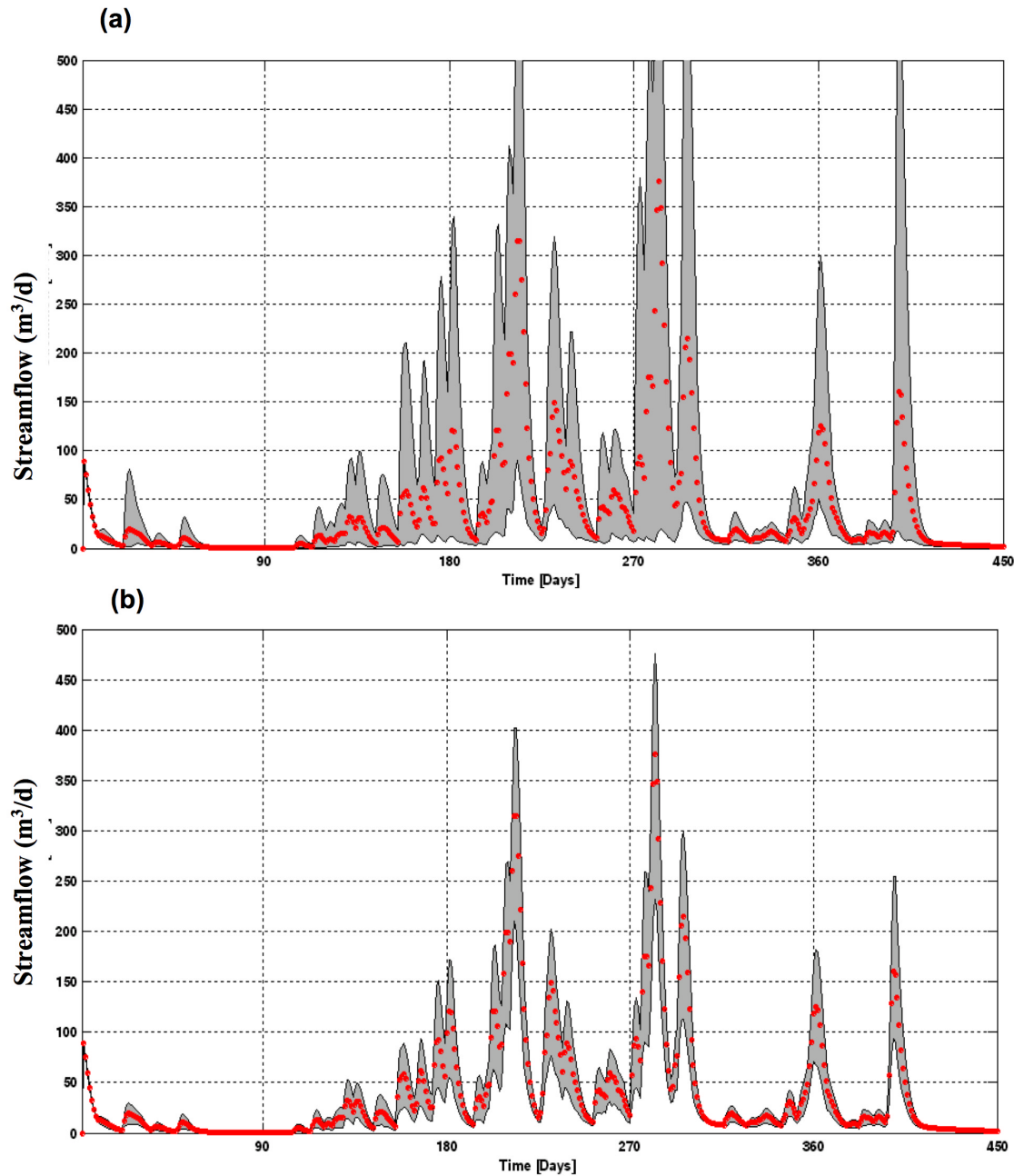


Figure 12. Uncertainty estimation of streamflow prediction corresponding to 95 percentile confidence using rainfall error propagation (a) fixed rainfall error 50% and (b) scale-dependent rainfall error according to equation (9). The red dots are mean of the 100 ensemble streamflow sequences simulated from satellite rainfall estimates.

generated streamflow values, while the lower bound can reach to the amount of no streamflow.

5. Summary and Conclusion

[23] As satellite-based precipitation estimates are increasingly applied to atmospheric and hydrological applications at various space-timescales, the estimation error itself and the effect of how the error propagates through models need to be evaluated as a whole so that the users have a certain degree of confidence while making decisions (Figure 1). Additionally, evaluation of error associated with precipitation products and

its propagation into model behavior is an indispensable element of evaluating data quality and improving hydrologic simulation techniques. Given these requirements, the aim of this paper is to foster the development of an end-to-end analysis framework that can quantify satellite-based precipitation estimation error and assess its influence on the uncertainty of hydrologic simulation.

[24] Satellite-based rainfall estimates from PERSIANN-CCS [Hong *et al.*, 2004] were used in this study. PERSIANN-CCS, a high-resolution precipitation estimation system operating at near real-time mode (<http://hydis8.eng.uci.edu/CCS/>), has been generating precipitation data at

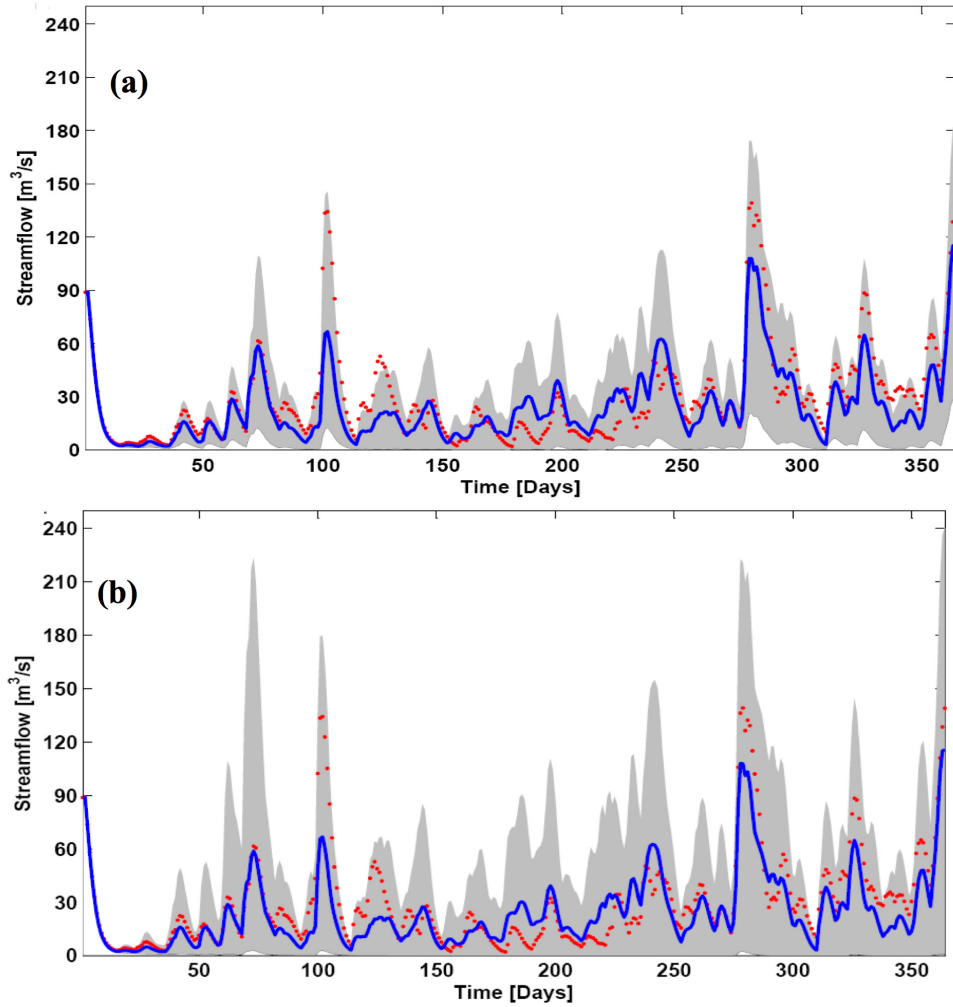


Figure 13. Comparison of runoff simulation generated from both stage IV precipitation radar measurement and satellite PERSIANN-CCS measurement at 1-year time span (1 July 2003 to 30 June 2004) (a) 66% confidence interval and (b) 95% confidence interval. Note that the red dots are streamflow generated from radar rainfall, the blue lines are synthetic mean of streamflow simulated from PERSIANN-CCS satellite rainfall estimates, and the gray areas are corresponding to confidence interval from 100 member ensemble simulation using satellite rainfall.

resolution ($0.04^\circ \times 0.04^\circ$ and 30-min time intervals) since 2000. The estimation error is quantified as the difference of satellite estimates and observations (equation (5)). It is further assumed that the uncertainty of satellite-based precipitation estimation error is a function of several factors, including spatial and temporal resolution of estimates, the estimated rain rates, and sampling frequency (equation (7)). Parameters of this scaling law equation were calibrated using PERSIANN-CCS precipitation estimates and NCEP gauge-corrected radar reference rainfall data (Figures 2–4 and Tables 1–3). The box plots of the 17 sets of parameters show that the parameters derived from different $5^\circ \times 5^\circ$ latitude-longitude grids are mostly consistent, with about 12%~16% of variation for one standard deviation of each parameter with respect to its mean value (Figure 5). However, for parameters b , c , and d , the range of values is more than 50% of their mean values, which suggests that the error of satellite-derived precipitation estimates is significantly region-dependent (Table 4). Figures 6 and 7 simulate the satellite estimation error as a function of rain intensity,

spatial scale, and temporal scale by implementing the optimally calibrated parameter set in equation (9). Just a reminder that the error quantified here should be interpreted as upper bound of ‘true error’ as discussed in the Appendix because NCEP gauge-corrected radar rainfall itself is not error free.

[25] The influence of the PERSIANN-CCS rainfall error on uncertainty of streamflow prediction is evaluated with Monte Carlo simulation in the Leaf River basin, Mississippi (Figure 8). By this approach, an ensemble of 100 precipitation data members is generated, as forcing input to a conceptual rainfall-runoff hydrologic model (Figure 9), and the resulting uncertainty in the predicted streamflow is quantified. Compared with the conventional error propagation procedure, i.e., fixed ratio error estimate (Figure 11c), our strategy not only provides more realistic quantification of precipitation estimation error but also offers improved uncertainty assessment of the error propagation from the precipitation input into the hydrological models (Figure 12). Finally, comparison of runoff simulation generated from

both stage IV radar precipitation measurement and satellite PERSIANN-CCS measurement is demonstrated in Figure 13. At the 95% confidence interval, radar-simulated streamflow values are contained by the uncertainty bound of satellite-simulated flow.

[26] The proposed uncertainty analysis framework in this study not only provides a general framework of satellite precipitation estimation error quantification procedure but also can assess its influence on the uncertainty of hydrologic prediction through Monte Carlo simulation of the error propagation. As a first attempt to quantify uncertainty of one of the major satellite-based precipitation data sets (PERSIANN-CCS) at fine scale ($0.04^\circ \times 0.04^\circ$ and hourly), the satellite rainfall error model (equation (7)) does not consider rainfall detection and false alarm probabilities. However, it is reported that these type of errors might compromise the accuracy of the error propagation into the hydrological model [Hossain and Anagnostou, 2006]. In our continuing effort to quantify the uncertainty of high-resolution satellite-based rainfall estimates, the error property of spatial-time integrated precipitation related to the undetected rainfall and false alarm scenarios will be investigated and embedded in the end-to-end uncertainty analysis framework report here.

Appendix A

[27] Ciach and Krajewski [1999] and Anagnostou *et al.* [1999] described the error variance separation issue in validation of radar rainfall estimates against ground gauge data. Similarly in the current study, reference data (R_{AT}^{ref}) are often used because of the absence of measurement of true rainfall R_{AT} . Therefore the reference error can be written as

$$(\hat{R}_{AT} - R_{AT}^{\text{ref}}) = (\hat{R}_{AT} - R_{AT}) - (R_{AT}^{\text{ref}} - R_{AT}) = \varepsilon - \varepsilon^{\text{ref}} \quad (\text{A1})$$

where R_{AT}^{ref} is the reference data such as gauge or radar and ε^{ref} represents the error associated with the reference data. The ε is always unknown due to the absence of the true measurement. Take the variance of both sides of equation (1):

$$\begin{aligned} \text{Var}[(\hat{R}_{AT} - R_{AT}^{\text{ref}})] &= \text{Var}[(\hat{R}_{AT} - R_{AT})] + \text{Var}[(R_{AT}^{\text{ref}} - R_{AT})] \\ &\quad - 2\text{Cov}[(\hat{R}_{AT} - R_{AT}), (R_{AT}^{\text{ref}} - R_{AT})] \\ &= \text{Var}[\varepsilon] + \text{Var}[\varepsilon^{\text{ref}}] - 2\text{Cov}[\varepsilon, \varepsilon^{\text{ref}}] \end{aligned} \quad (\text{A2})$$

where Var denotes variance and Cov denotes covariance. Assume that ε and ε^{ref} are uncorrelated because satellite-based rainfall estimation algorithms are usually independent from gauge and radar rainfall measurements. The reference error variance therefore can be written as

$$\text{Var}[(\hat{R}_{AT} - R_{AT}^{\text{ref}})] = \text{Var}[\varepsilon] + \text{Var}[\varepsilon^{\text{ref}}] \quad (\text{A3})$$

$\text{Var}[\varepsilon]$ can be assessed using independent reference data (i.e., radar or gauge rainfall) if the error characteristics of reference data $\text{Var}[\varepsilon^{\text{ref}}]$ are known or derivable. In this study, the reference error ($\hat{R}_{AT} - R_{AT}^{\text{ref}}$) is used to approximate $(\hat{R}_{AT} - R_{AT})$ because (1) the R_{AT} is usually unavailable and (2) the reference error is the relaxant representation of true error (upper bound) because the $\text{Var}[(\hat{R}_{AT} - R_{AT}^{\text{ref}})]$ is the upper bound of $\text{Var}[\varepsilon]$ [Gebremichael *et al.*, 2003].

[28] **Acknowledgments.** Partial support for this research is from NASA-EOS grant (NA56GPO185) and NASA TRMM project (NAG5-7716). The authors would like to thank Steve Burges and the other two anonymous reviewers for their constructive comments.

References

- Adler, F. R., et al. (2003), The version-2 Global Precipitation Climatology Project (GPCP) monthly precipitation analysis (1979–present), *J. Hydrometeorol.*, **4**, 1147–1167.
- Anagnostou, E. N., W. F. Krajewski, and J. A. Smith (1999), Uncertainty quantification of mean-area radar rainfall estimates, *J. Atmos. Oceanic Technol.*, **16**(2), 206–215.
- Ba, M., and A. Gruber (2001), GOES Multispectral Rainfall Algorithm (GMSRA), *J. Appl. Meteorol.*, **29**, 1120–1135.
- Bellerby, T., M. Todd, D. Kniveton, and C. Kidd (2000), Rainfall estimation from a combination of TRMM precipitation radar and GOES multispectral satellite imagery through the use of an artificial neural network, *J. Appl. Meteorol.*, **39**, 2115–2128.
- Boyle, D. P., H. V. Gupta, and S. Sorooshian (2000), Toward improved calibration of hydrological models: Combining the strengths of manual and automatic methods, *Water Resour. Res.*, **36**, 3663–3674.
- Boyle, D. P., H. V. Gupta, S. Sorooshian, V. Koren, Z. Zhang, and M. Smith (2001), Toward improved streamflow forecasts: Value of semi-distributed modeling, *Water Resour. Res.*, **37**, 2749–2760.
- Burges, S. J. (2003), Process representation, measurements, data quality, and criteria for parameter estimation of watershed models, in *Calibration of Watershed Models*, *Water Sci. Appl.*, vol. 6, edited by Q. Duan *et al.*, pp. 283–299, AGU, Washington, D. C.
- Carpenter, T. M., and K. P. Georgakakos (2004), Continuous streamflow simulation with the HRCDHM distributed hydrologic model, *J. Hydrol.*, **298**, 61–79.
- Ciach, G. J., and W. F. Krajewski (1999), On the estimation of radar rainfall error variance, *Adv. Water Resour.*, **22**, 585–595.
- Ciach, G. J., E. Habib, and W. F. Krajewski (2003), Zero-covariance hypothesis in the Error Variance Separation method of radar rainfall verification, *Adv. Water Resour.*, **26**, 673–680.
- Gebremichael, M., W. F. Krajewski, M. Morrissey, D. Langerud, G. J. Huffman, and R. Adler (2003), Error uncertainty analysis of GPCP monthly rainfall products: A data-based simulation study, *J. Appl. Meteorol.*, **42**, 1837–1848.
- Hong, Y., K. Hsu, X. Gao, and S. Sorooshian (2004), Precipitation estimation from remotely sensed imagery using Artificial Neural Network-Cloud Classification System, *J. Appl. Meteorol.*, **43**, 1834–1853.
- Hong, Y., K. Hsu, S. Sorooshian, and X. Gao (2005), Self-Organizing Nonlinear Output (SONO): A neural network suitable for cloud patch-based rainfall estimation from satellite imagery at small scales, *Water Resour. Res.*, **41**, W03008, doi:10.1029/2004WR003142.
- Hossain, F., and E. N. Anagnostou (2004), Assessment of current passive-microwave- and infrared-based satellite rainfall remote sensing for flood prediction, *J. Geophys. Res.*, **109**, D07102, doi:10.1029/2003JD003986.
- Hossain, F., and E. N. Anagnostou (2006), A two-dimensional satellite rainfall error model, *IEEE Trans. Geosci. Remote Sens.*, in press.
- Hossain, F., E. N. Anagnostou, and T. Dinku (2004), Sensitivity analyses of satellite rainfall retrieval and sampling error on flood prediction uncertainty, *IEEE Trans. Geosci. Remote Sens.*, **42**(1), 130–139.
- Hsu, K., X. Gao, S. Sorooshian, and H. V. Gupta (1997), Precipitation estimation from remotely sensed information using artificial neural networks, *J. Appl. Meteorol.*, **36**, 1176–1190.
- Huffman, G. J., R. Adler, M. Morrissey, D. Bolvin, S. Curtis, R. Joyce, B. McGavock, and J. Susskind (2001), Global precipitation at one-degree daily resolution from multisatellite observations, *J. Hydrometeorol.*, **2**, 36–50.
- Huffman, J. (1997), Estimates of root-mean-square random error for finite samples of estimated precipitation, *J. Appl. Meteorol.*, **36**, 1191–2101.
- Joyce, R. J., J. E. Janowiak, P. A. Arkin, and P. Xie (2004), CMORPH: A method that produces global precipitation estimates from passive microwave and infrared data at high spatial and temporal resolution, *J. Hydrometeorol.*, **5**, 487–503.
- Kidd, C., D. R. Kniveton, M. C. Todd, and T. J. Bellerby (2003), Satellite rainfall estimation using combined passive microwave and infrared algorithms, *J. Hydrometeorol.*, **4**, 1088–1104.
- Krajewski, W. F., V. Lakshmi, K. P. Georgakakos, and S. C. Jain (1991), A Monte -Carlo study of rainfall sampling effect on a distributed catchment model, *Water Resour. Res.*, **27**(1), 119–128.

- Krajewski, W. F., G. J. Ciach, J. R. McCollum, and C. Bacotiu (2000), Initial validation of the Global Precipitation Climatology Project over the United States, *J. Appl. Meteorol.*, **39**, 1071–1086.
- Krzysztofowicz, R. (1999), Bayesian theory of probabilistic forecasting via deterministic hydrologic model, *Water Resour. Res.*, **35**(9), 2739–2750.
- Kuligowski, R. J. (2002), A self-calibrating real-time GOES rainfall algorithm for short-term rainfall estimates, *J. Hydrometeorol.*, **3**, 112–130.
- Li, Q., R. L. Bras, and D. Veneziano (1996), Analysis of Darwin rainfall data: Implications on sampling strategy, *J. Appl. Meteorol.*, **35**, 372–385.
- Li, Q., R. Ferraro, and N. C. Grody (1998), Detailed analysis of the error associated with the rainfall retrieved by the NOAA/NESDIS SSM/I rainfall algorithm: 1. Tropical oceanic rainfall, *J. Geophys. Res.*, **103**, 11,419–11,427.
- McCollum, J. R., and W. F. Krajewski (1998), Investigations of error sources of the Global Precipitation Climatology Project emission algorithm, *J. Geophys. Res.*, **103**, 28,711–28,719.
- Miller, S. W., P. A. Arkin, and R. Joyce (2001), A combined microwave/infrared rain rate algorithm, *Int. J. Remote Sens.*, **22**(17), 3285–3307.
- Moore, R. J. (1985), The probability-distributed principle and runoff production at point and basin scales, *Hydrol. Sci. J.*, **30**(2), 273–297.
- Moradkhani, H., K. Hsu, H. V. Gupta, and S. Sorooshian (2005a), Uncertainty assessment of hydrologic model states and parameters: Sequential data assimilation using particle filter, *Water Resour. Res.*, **41**, W05012, doi:10.1029/2004WR003604.
- Moradkhani, H., S. Sorooshian, H. V. Gupta, and P. Houser (2005b), Dual state-parameter estimation of hydrological models using ensemble Kalman filter, *J. Adv. Water Res.*, **28**, 2135–2147.
- Rudolf, B. (1993), Management and analysis of precipitation data on a routine basis, in *Proceedings of the International WMO/IAHS/ETH Symposium on Precipitation and Evaporation*, vol. 1, edited by M. Lapin and B. Sevruk, pp. 69–76, Slovak Hydrometeorol. Inst., Bratislava, Slovakia.
- Sorooshian, S., K. Hsu, X. Gao, H. V. Gupta, B. Imam, and D. Braithwaite (2000), Evolution of the PERSIANN system satellite-based estimates of tropical rainfall, *Bull. Am. Meteorol. Soc.*, **81**(9), 2035–2046.
- Steiner, M. (1996), Uncertainty of estimates of monthly areal rainfall for temporally sparse remote observations, *Water Resour. Res.*, **32**, 373–388.
- Steiner, M., J. A. Smith, S. J. Burges, C. V. Alonso, and R. W. Darden (1999), Effect of bias adjustment and rain gauge data quality control on radar rainfall estimation, *Water Resour. Res.*, **35**, 2487–2503.
- Steiner, M., T. L. Bell, Y. Zhang, and E. F. Wood (2003), Comparison of two methods for estimating the sampling-related uncertainty of satellite rainfall averages based on a large radar data set, *J. Clim.*, **16**, 3759–3778.
- Xie, P., J. E. Janowiak, P. A. Arkin, R. F. Adler, A. Gruber, R. Ferraro, G. J. Huffman, and S. Curtis (2003), GPCP pentad precipitation analyses: An experimental data set based on gauge observations and satellite estimates, *J. Clim.*, **16**, 2197–2214.

Y. Hong, NASA Goddard Space Flight Center, Mail Stop 613.1, Greenbelt, MD 20771, USA. (yanghong@agnes.gsfc.nasa.gov)

K.-L. Hsu, H. Moradkhani, and S. Sorooshian, Center for Hydrometeorology and Remote Sensing, Department of Civil and Environmental Engineering, University of California, Irvine, CA 92697, USA.